Applied Materials Today 30 (2023) 101713

Contents lists available at ScienceDirect

Applied Materials Today

journal homepage: www.elsevier.com/locate/apmt

Glucose sensing by field-effect transistors based on interfacial hydrogelation of self-assembled peptide

Tengyan Xu [a,1], Huihui Ren [b,c,1], Yu Fang [a], Kun Liang [b,c], Hongyue Zhang [a], Dingwei Li [b,c], Yitong Chen [b,c], Bowen Zhu [b,2], Huaimin Wang [a,*]

[a] Key Laboratory of Precise Synthesis of Functional Molecules of Zhejiang Province, School of Science, Institute of Natural Sciences, Westlake Institute for Advanced Study, Westlake University, 18 Shilongshan Road, Hangzhou, Zhejiang 310024, China
[b] Key Laboratory of 3D Micro/Nano Fabrication and Characterization of Zhejiang Province, School of Engineering, Westlake University, Hangzhou, Zhejiang 310024, China
[c] School of Materials Science and Engineering, Zhejiang University, Hangzhou 310027, China

ARTICLE INFO

Keywords:
Self-assembly
Hydrogel
Surface induced hydrogelation
Field-effect transistor-based biosensor
Wearable device

ABSTRACT

Interfacial hydrogelation of peptides gated on the semiconductor channel has yet to be explored in surface chemistry and field-effect transistor-based biosensors (bio-FETs). This work reports the first example of peptidic hydrogel gated bio-FET by surface assisted self-assembly for label-free and real-time monitoring of the glucose with low limit of detection, excellent sensitivity, and good stability in mouse serum. The boric acid-containing peptide forms a hydrogel layer on the surface of In_2O_3, which interacts with glucose reversibly and generates boronate anions to influence the semiconductor's conductivity. The results also indicate the superiority of hydrogel gated bio-FET for real-time monitoring of glucose in complex environments and serve as a wearable device. This work illustrates a simple and fundamental strategy for integrating peptidic hydrogel with bio-FET for the real-time detection of analytes.

1. Introduction

Field-effect transistor-based biosensor (bio-FET) has been developed as a label-free, miniaturized, and intrinsic signal amplification transducer for biological detection with extreme environmental sensitivity and ultra-low power requirements [1,2]. Unlike common amperometry sensors that require high oxidation potential depending on target molecules and working electrodes, bio-FET is based on electrostatic gating of semiconductor channels via target-receptor interactions, inducing variations in transconductance and the carrier concentration, which could potentially respond to almost all charged molecules [3–7]. Typically, even low receptor occupancy of target molecules could affect channel conductance through capacitive coupling [8–10]. However, most biological receptors (e.g., enzymes) could lose their activity rapidly after incubation on the FET with changes in the surrounding environment [11]. Moreover, although enzymatic biosensors exhibit the advantages of good affinity between the analyte and receptors, chemical instability, complicated enzyme immobilization and rigorous operating environments (pH and temperature) limit their future clinic and wearable application [12–15]. Moreover, in conventional non-enzymatic bio-FETs, the nanoscale channels and source/drain electrodes in devices with self-assembled monolayers (SAMs) are often exposed to electrolytes environments, where the background signals will be distracted by interference in the electrolyte, which leads to poor stability over long-term measurement [16,17]. Another common limiting factor of enzyme-based sensors is oxygen-consuming, which will lead to errors in sensing response and an upper limit of linearity [18]. Thus, the ideal strategy for improving the bio-FET is to provide a biomimetic environment for maintaining the stability of biomolecules and realize long-term stability and low-power dissipation for continuous measurement, which is hard to achieve and remains challenging.

Molecular self-assembly is a powerful strategy and spontaneous process to organize biomolecules, nanometer-scale or beyond ordered structures at the interface through a variety of stimuli (pH, temperature, ionic stress, enzyme, etc.) [19,20], which has been applied for creating functional materials with emerging properties in the field of health care

* Corresponding author.
E-mail address: wanghuaimin@westlake.edu.cn (H. Wang).
[1] These authors contributed equally to this work.
[2] Co-corresponding author: zhubowen@westlake.edu.cn

https://doi.org/10.1016/j.apmt.2022.101713
Received 19 August 2022; Received in revised form 18 November 2022; Accepted 1 December 2022
Available online 11 December 2022

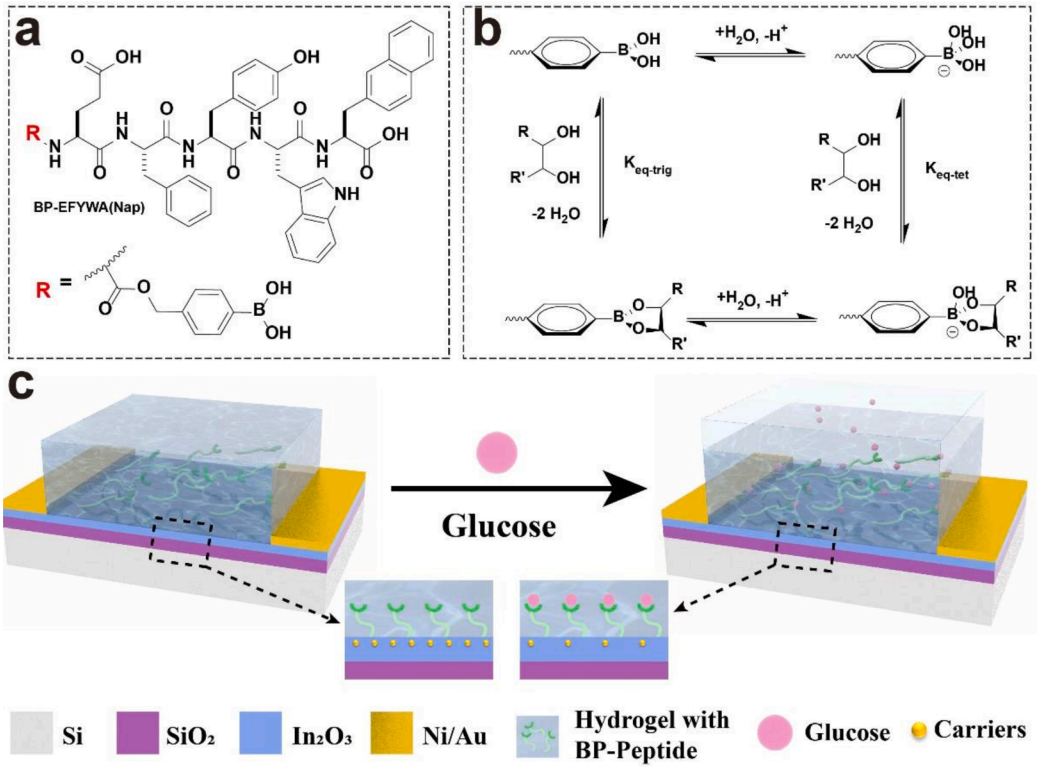

Fig. 1. (a) Molecular structure of BP-EFYWA(Nap). (b) Detection mechanism and the equilibrium of phenylboronic acid when exposure to glucose. (c) Schematic illustration of localized self-assembly of molecular hydrogel on In_2O_3 based bio-FET to various [glucose].

[21,22]. Recent investigations of supramolecular hydrogel and surface-induced effect illustrated that localized molecular self-assembly on a surface exhibited unique advantages in several systems [23,24]. Moreover, the hydrogel could provide the semi-wet microenvironment for many biological events and is suitable for overcoming the drawbacks of conventional biosensors [25]. However, localized molecular self-assembly of peptidic hydrogel on the bio-FET system is less explored due to the complexity, stability of surface modification, and higher detection sensitivity. Very recently, surface assisted self-assembly showed the promise to modify different surfaces [26,27]. For example, enzyme localized molecular self-assembly is an efficient strategy to control cell fate by enzyme induced chemical reaction locally [28]. The surface hydrogelation of tripeptide on platelets could inhibit platelet aggregation [29]. Loïc Jierry and co-workers also developed enzyme-assisted self-assembly of peptides at the walls of a supporting porous material for continuous flow chemistry [30].

Inspired by the above pioneering work, we hypothesized that interfacial hydrogelation gated on bio-FET could be a general strategy to overcome the drawbacks of bio-FET sensors (e.g., stability and sensitivity of biomolecules in complex conditions). The results show that the designed molecule BP-EFYWA(Nap) (Fig. 1a) self-assembles to form a nanofibrous network on the surface of the In_2O_3 channel through non-covalent interactions. The display of phenylboronic acid on nanofibers could bind to the analyte (e.g., glucose). The presence of glucose in complex conditions (phosphate buffer saline and blood from mice) pushes the reaction to the right and generates boronate anions (Fig. 1b), which could modulate the carriers transport of semiconductor channel. We also demonstrated that the bio-FET sensor could design to form a wearable device for real-time monitoring. Overall, a novel localized self-assembled peptide was developed to form analyte-responsive hydrogel on the surface of the FET sensor, providing a simple and fundamental strategy for real-time blood glucose detection. The self-assembling peptides functionalized bio-FETs with specific recognition motifs have great potential applications in detecting disease-related biological analytes.

2. Methods and materials

2.1. Materials

Fmoc-amino acids were obtained from GL Biochem (Shanghai). 4-Hydroxymethylphenyl boronic acid was purchased from Bide Pharmatech Ltd (Shanghai). 1,3-propanediol was brought from D&B Chemical Technology CO. Ltd (Shanghai). 2-Cl-trityl chloride resin was obtained from Nankai Resin Co. Ltd. (Tianjin). All the other starting materials were obtained from Alfa (Beijing). Commercially available reagents were used without further purification unless noted otherwise. Deionized water was used for all experiments. All other chemicals were reagent grade or better.

The synthesized compounds were characterized using ^{1}H NMR (Bruker AVANCE NEO 500 MHz). HPLC was conducted at Agilent 1260 Infinity II Manual Preparative Liquid Chromatography system using a C18 RP column with CH_3CN (0.1% of TFA) and water (0.1% of TFA) as the eluents. LC-MS was conducted at the Agilent InfinityLab LC/MSD system.

2.2. Peptide synthesis

H_2N-EFYWA(Nap) was synthesized by solid-phase peptide synthesis (SPPS) using 2-chlorotrityl chloride resin, and the corresponding N-Fmoc protected amino acids with side chains properly protected by different groups. Firstly, the C-terminal of the first amino acid was conjugated on the resin. Anhydrous N, N'-dimethyl formamide (DMF) containing 20% piperidine was used to remove Fmoc protected group. To couple the next amino acid to the free amino group, O-(Benzotriazol-1-yl)-N, N, N', N'-tetramethyluronium hexafluorophosphate (HBTU) was used as coupling reagent. The growth of the peptide chain was according to the established Fmoc SPPS protocol. After the last coupling

step, excessive reagents were removed by a single DMF wash for 5 min (5 mL per gram of resin), followed by five steps of washing using DCM for 2 min (5 mL per gram of resin). The peptide was cleaved using 95% of trifluoroacetic acid (TFA) with 2.5% of triisopropylsilane (TIS) and 2.5% of H_2O for 30 min. 20 mL per gram of resin of ice-cold diethyl ether was then added to cleavage reagent. The resulting precipitate was centrifuged for 10 min at 4 °C at 5000 rpm. Afterward the supernatant was decanted, and the resulting solid was dissolved in H_2O/CH_3CN (1:1) for HPLC separation using CH_3CN and H_2O containing 0.1% of TFA as eluents.

2.3. Preparation of 4-(1,3,2-dioxaborinan-2-yl) phenyl) methanol

2.0 g of 4-Hydroxymethylphenyl boronic acid and 1.0 g of 1,3-propanediol were dissolved in 40 mL of dried tetrahydrofuran (THF) at room temperature. The reaction mixture was stirred and reacted for 72 h. The reaction mixture was evaporated under decompression to remove the solvent and purified with a silica-gel chromatography (Petroleum ether/ethyl acetate = 6/4) to obtain the 4-(1,3,2-dioxaborinan-2-yl) phenyl) methanol which was a colorless viscous liquid.

2.4. Preparation of BP-EFYWA(Nap)

195 mg of 4-(1,3,2-dioxaborinan-2-yl) phenyl) methanol and 395 mg of N, N'-Disuccinimidyl carbonate (DSC) were dissolved in 30 mL of acetonitrile, 400 μL of trimethylamine (TEA) was added, and the mixture was stirred at room temperature for 1.5 h under nitrogen protection. After the TLC monitors the completion of the reaction, add 50 mL of chloroform to dilute, wash the organic layer 3 times with distilled water. The resulting solution was dried with anhydrous sodium sulfate, and then filtered to obtain a clarified solution. The organic solvent was removed by decompression to obtain a colorless viscous liquid. 19.3 mg of the above intermediates were dissolved in 10 mL THF and added to an aqueous solution (1 mL) containing 49 mg H_2N-EFYWA(Nap) and 100 μL TEA. The mixture was stirred overnight at room temperature, then decompressed to remove the organic solvent, 1 N HCl aqueous solution was used to adjust the solution pH to 3. We can find that the solution becomes cloudy, then centrifuge for 5 min (5000 rpm) to remove the supernatant and obtain the final product. Afterward the resulting product was dissolved in H_2O/CH_3CN (1:1) for HPLC separation using CH_3CN and H_2O containing 0.1% of TFA as eluents.

2.5. Hydrogel formation

BP-EFYWA(Nap) was prepared at a final concentration of 3.0 mg mL^{-1} in aqueous solution (pH = 7.0), add 1 N HCl to adjust the pH to 5.5 and incubated at room temperature, a transparent gel would form within 4 h.

H_2N-EFYWA(Nap) was prepared at a final concentration of 2.5 mg mL^{-1} (molar concentration was the same as BP-EFYWA(Nap)) in aqueous solution (pH = 7.0). After adding HCl (1 N) to adjust the final pH to 5.5, a transparent gel could form within 3 h at room temperature.

2.6. TEM

BP-EFYWA(Nap) were prepared at a final concentration of 3.0 mg mL^{-1} in aqueous solution, add 1N NaOH to adjust the pH to 7.0. They were divided into two groups; one group was adjusted to pH 5.5 to form a hydrogel with 1N HCl. Negative staining technique was used to observe the TEM images of micro structure in solution. A micropipette was used to load 10 μL of sample solution to a carbon-coated copper grid, the excess solution was removed by a piece of filter paper. The deionized water was then used to rinse grid, 10 μL of UA stain the sample for 1.5 min, rinse the grid with deionized water again and then conducted on a Talos L120C system, operating at 120 kV.

2.7. Critical aggregation concentration

The CAC values of BP-EFYWA(Nap) at pH 7.0 and 5.5 were determined by dynamic light scattering (DLS). Solutions containing different concentration of peptide derivatives were tested and the light scattering intensity was recorded for each concentration analyzed, each concentration was repeated three times. DLS was performed on a laser light scattering spectrometer (BI-200SM, Brookhaven Instruments), the lower CAC values representative better assembly capacity.

2.8. Circular dichroism (CD)

CD was measured by an Applied Photophysics Ltd (Chirascan V100) system. All the samples were placed into quartz spectrophotometer cell and the wavelength range was from 190 to 260 nm and the step was 1 nm.

2.9. Rheology

Rheology test was carried out on an ARES-G2 (TA instrument) system, 25 mm parallel plates were used during the experiment at the gap of 500 μm. In the process of dynamic frequency scanning, the obtained hydrogel was transferred to the test platform with a pipette, the fixed strain is 0.5%, and the change of elastic modulus (G') and viscous modulus (G'') of the colloid during scanning in the range of frequency from 100 to 0.01 Hz was tested according to the set program. The gels were then characterized by dynamic strain sweep with a fixed frequency of 1 Hz, test the changes in elastic modulus (G') and viscous modulus (G'') of the hydrogel when the strain% is changed within the range of 0.01%−100%.

2.10. Preparation of precursor solution

0.1 M In_2O_3 precursor solution was prepared by dissolving 0.30 g Indium (III) nitrate hydrate ($In(NO_3)_3{\cdot}xH_2O$, 99.999%, Sigma Aldrich) into a mixed solvent of 10 mL 2-methoxyethanol (2-ME, 99.3%, Alfa Aesar), 100 μL, acetylacetone (AcAc, 99%, Alfa Aesar) and 35 μL ammonium hydroxide ($NH_3{\cdot}H_2O$, 28%, Alfa Aesar). The prepared precursor solution was stirred at room temperature for 24 h, and then filtered via a nylon syringe filter with the pore size of 0.2 μm prior to use. AcAc and $NH_3{\cdot}H_2O$ as additives were introduced in precursor solution to boost combustion reaction and thus optimize the electrical performances of solution-processed metal oxide thin film [31].

2.11. Device fabrication

The FET devices were fabricated with a bottom-gate, top-contact (BGTC) structure on the highly doped silicon substrate with 100 nm thick SiO_2 dielectric layer (Silicon Valley Microelectronics, Inc). The Si/SiO_2 substrates were firstly ultrasonicated by acetone, isopropanol, and deionized (DI) water for 5 min, respectively. Then the wafers were cleaned by oxygen plasma for 5 min to render the surfaces hydrophilic prior to spin-coating processes. Subsequently, as reported before, the In_2O_3 channels were formed by direct light patterning (DLP) technology [32]. Typically, the 0.1 M In_2O_3 precursor was spun on Si/SiO_2 wafers 3000 r/min for 30 s, following by pre-baked at 100 °C in the air for 1 min to remove organic solvents. Next, the prepared samples were exposed to deep ultraviolet (DUV) irradiation via a shadow mask for 10 min to trigger photochemical activation event of the In_2O_3 thin film. The mixed solution (acetic acid: methanol = 1: 20, v: v) was applied to UV-treated substrates, and finally the unexposed areas were etched, leaving the In_2O_3 pattern film, following by annealing at 300 °C in the air for 1 h. The Ni and Au with the thickness of 8/30 nm or 50 nm Al were sequentially deposited as the source and drain interdigital electrodes via shadow masks by the thermal evaporation, forming a channel width (W) and length (L) of 7500 μm and 200 μm, respectively. For glucose sensing,

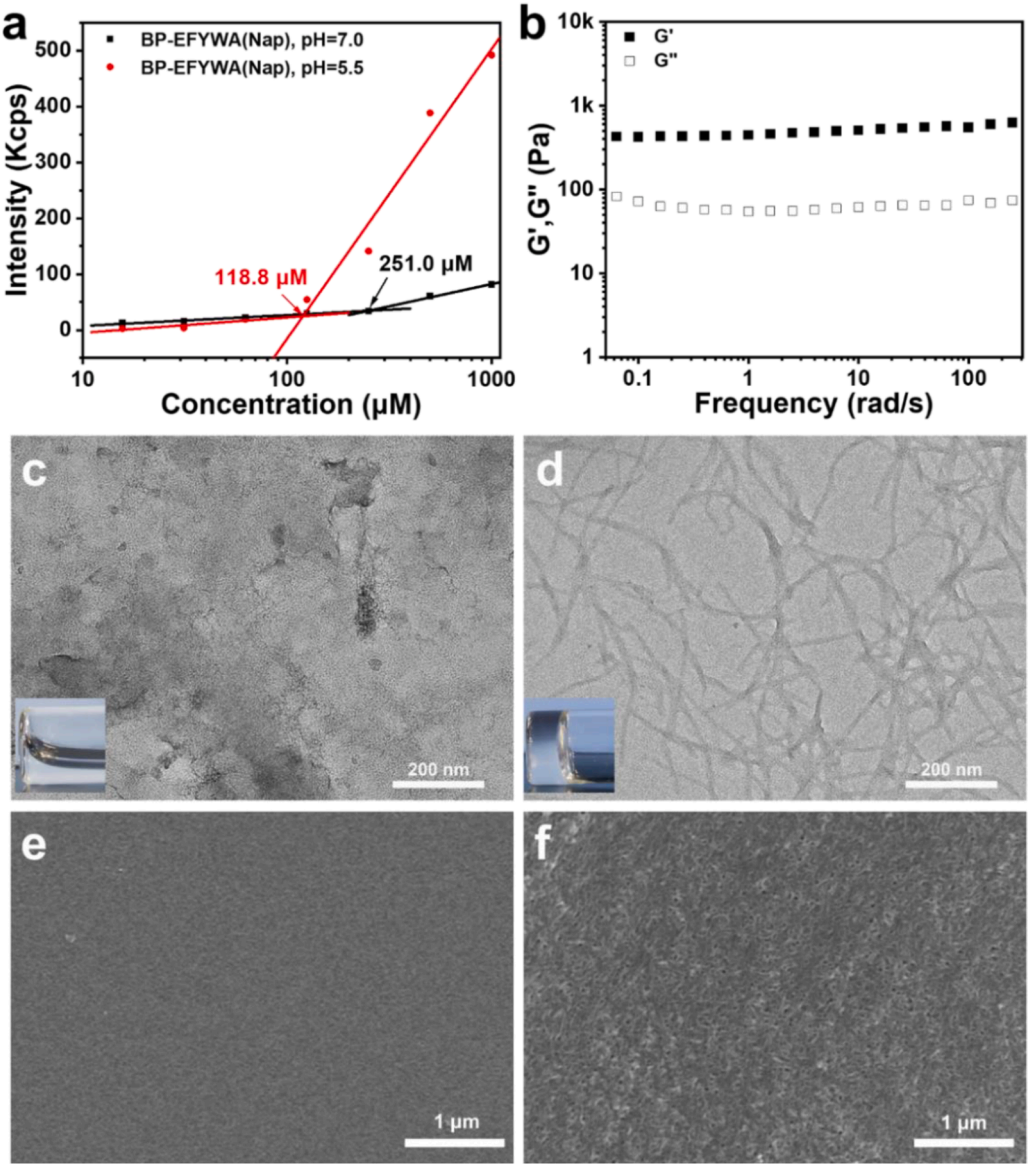

Fig. 2. (a) CAC values of BP-EFYWA(Nap) at pH 7.0 and 5.5. (b) Dynamic frequency sweep of BP-EFYWA(Nap) hydrogel at the strain value of 0.5%. TEM images of BP-EFYWA(Nap) (0.3 wt.%) (c) at pH 7.0 and (d) pH 5.5 in an aqueous solution. Inserts are the corresponding optical image of vial test. SEM images of (e) native surface of bio-FET and (f) hydrogel formation on the bio-FET surface.

the In_2O_3 FETs were firstly modified by APTES layer, where the devices were incubated in 5% (3-aminopropyl) triethoxysilane (APTES, 98%, Alfa Aesar) ethanol solution for 10 min, following by cleaning with ethanol and DI water for 3 times. Next, 50 μL 0.3% BP-EFYWA(Nap) aqueous solution with pH 5.5 was added to the prepared device and let stand for 4 h to form the hydrogel.

2.12. Flexible device fabrication

Each ultrathin ~2.9 μm-thick polyimide (Sigma Aldrich, PI) film was attached to the glasses used as conformal flexible substrates. PI solution was spin-coating on cleaned glass substrates at 1000 rpm for 60 s in N_2 inert gas ambient. The prepared substrates were annealed in four steps: samples were prebaked at 150 °C, 200 °C, and 250 °C each for 30 min, and annealed at 300 °C for 1 h [9,33]. Next, 0.2 M aluminum (III) nitrate nonahydrate ($Al(NO_3)_3{\cdot}9H_2O$, 99.997%, Sigma Aldrich) solution in 2-ME was spun on prepared PI films and baked at 300 °C for 1 h in the air environment to fill the gaps [34]. The fabrication processes of the channel layer and S/D interdigital electrodes is the same as that on silicon wafers substrate. After that, the In_2O_3 FETs on PI films were carried out mechanically exfoliated from the carrier glasses.

2.13. Characterization of FETs

The electrical characteristics of FETs and bio-FETs were measured in dry and liquid condition using semiconductor parameter analyzer (Keithley 4200 SCS) and/or source meter (Agilent B2912A) combined with probe station system. The saturation mobility (μ_{sat}) and sub-threshold swing (SS) were expressed as

$$\mu_{sat} = \frac{2L}{WC_{ox}}\left(\frac{\partial\sqrt{I_{ds}}}{\partial V_{gs}}\right)^2 \quad (1)$$

, and

$$SS = \frac{\partial V_{gs}}{\partial(\log_{10} I_{ds})} \quad (2)$$

where W and L are the channel width and length of the FETs. C_{ox} is the

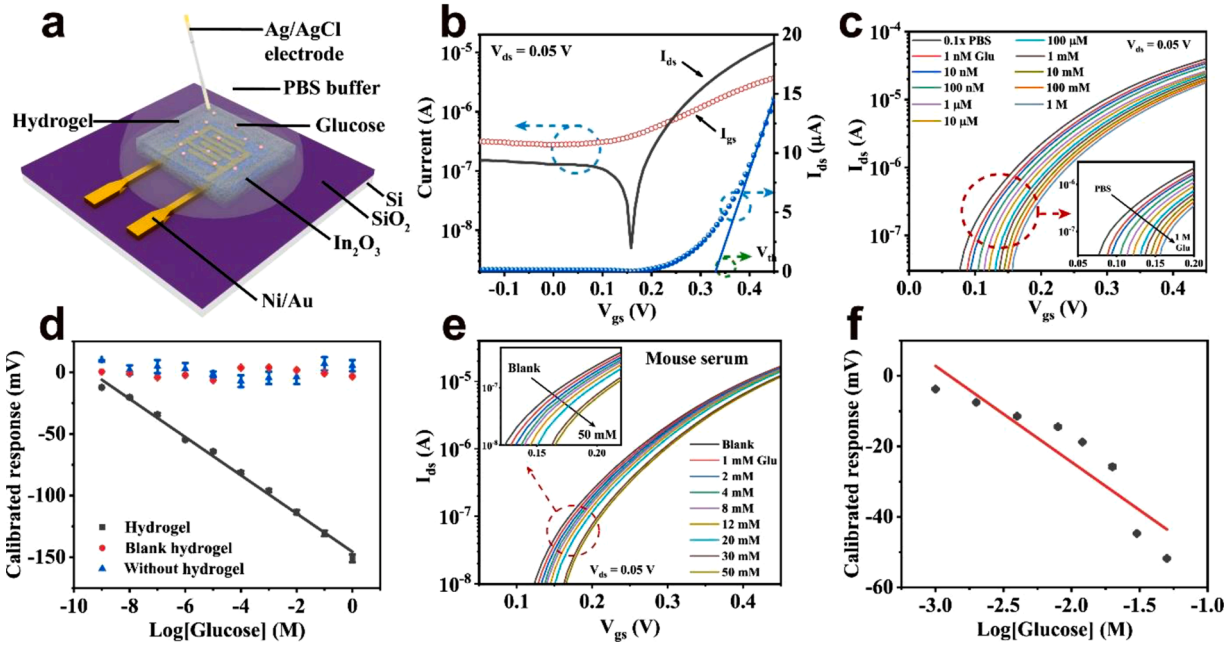

Fig. 3. (a) Device set up of In_2O_3 FETs with the channel regions of 4640/200 μm (*W/L*), where the In_2O_3 layer (blue color) is below the hydrogel (transparent filamentous structure), and the hydrogel covers the entire surface of the In_2O_3 channel. The Ag/AgCl reference electrode serves as the liquid gate. (b) Transfer curves of the devices in 1 M glucose solution. Black solid line refers to I_{ds} curve in logarithmic scale; blue solid circles refer to I_{ds} curve in linear scale; red open circles refer to I_{gs} curve. (c) Typical transfer curves of hydrogel gated FETs exposure of the various concentrations of glucose. (d) The average relationship between calibrated response and [glucose] in logarithmic scale for hydrogel (H_2N-EFYWA(Nap)) encoded In_2O_3 FETs, blank hydrogel indicates the hydrogel without boric acid group gated devices and bare In_2O_3 FETs ($n = 3$). (e) Typical transfer characteristics for glucose (1 mM to 50 mM) responses in mouse serum of hydrogel gated bio-FETs. (f) The sensor response shift as a function of [glucose] in logarithmic scale in mouse serum samples ($n = 3$).

capacitance of the gate dielectric (SiO_2) layer.

3. Results and discussion

3.1. Design, synthesis and characterization of interfacial hydrogelation of self-assembled peptide

To investigate the interfacial hydrogelation gated on bio-FET for non-enzyme detection of glucose. We designed BP-EFYWA(Nap) for the following rationales: (1) the naphthyl group provides strong aromatic-aromatic interactions to promote the self-assembly systems [35]; (2) The tripeptide WYF has the excellent self-assembly properties to form regular nanostructures through π-π stacking [36,37]; (3) Glutamic acid serves as a hydrophilic part to balance the solubility of the whole system; (4) Boric acid group interacts with glucose reversibly and generates boronate anions (Fig. 1b) after interacting with glucose for electronic detection [38]. After exposure to glucose, a boron acid molecule with a tertiary state (electron-deficient structure) transfers to the quaternary state (electron-rich structure) [39]. Therefore, the bio-FET transmits signals by reducing the carries in In_2O_3 channels upon target binding, owing to the electrostatic repulsion of charge carriers (Fig. 1c). Such a design allows us to generate the nanofibrous hydrogel on the surface of In_2O_3 channel and responds to the analyte through multivalent interactions. After synthesizing H_2N-EFYWA(Nap) by standard Fmoc based solid-phase peptide synthesis, phenylboronic acid-activated ester (Scheme S1) reacts with the peptide in the liquid phase to generate BP-EFYWA(Nap) and is purified by reverse phase HPLC, and verified by LC-MS and NMR (Figs. S4 and S5).

Fig. 2a shows that the critical aggregation concentration (CAC) values of BP-EFYWA(Nap) at pH 7.0 and 5.5 are 251.0 μM and 118.8 μM, respectively indicating that BP-EFYWA(Nap) has better self-assembly ability at pH 5.5. Since BP-EFYWA(Nap) contains a carboxyl and boronic acid group, it forms a transparent solution in an aqueous solution (pH = 7.0). After adjusting the final pH to 5.5, the protonation of the carboxyl group provided additional hydrogen bonding, resulting in the change of the hydrophilic-hydrophobic balance of the peptide, which could promote the further self-assembly of the BP-EFYWA(Nap) to form a transparent hydrogel (Insert images in Fig. 2c and 2d). TEM results revealed that BP-EFYWA(Nap) forms random clumps, which transform into three-dimensional nanofibrous networks with a diameter of about 12 nm (Fig. 2c and 2d). Cryo-EM experiments also indicate that the nanofibers of the hydrogel exhibit similar morphologies and diameter (Fig. S6). The rheological result (Figs. 2b and S7) showed that the elasticity (G') of BP-EFYWA(Nap) is higher than viscosity (G'') values and has weak frequency dependency between 0.01 and 100 Hz, suggesting BP-EFYWA(Nap) forms a stable hydrogel.

3.2. Hydrogel gated FET sensor for the detection of glucose in PBS buffer and mouse serum samples

To examine the localized molecular self-assembly of BP-EFYWA (Nap) on FET surface, we used ultrathin In_2O_3 (~6 nm) to serve as a channel layer for constructing FET architecture (Fig. S8) [40]. The results show that BP-EFYWA(Nap) self-assembles on the prepared In_2O_3 channel to form an active hydrogel layer through surface-induced hydrogelation, as evidenced by the scanning electron microscope (SEM) images (Fig. 2e and 2f). As shown in Fig. 3a and 3b, the hydrogel gated FETs (50 μL of peptide hydrogel deposited on its surface, Fig. S9) could operate normally in harsh conditions of the buffer containing 1 M glucose (Fig. S10), revealing improved electrical characteristics with a low *SS* of 66.6 mV dec^{-1} and a low operation voltage (0.05 V). The representative transfer curves (I_{ds}-$V_{Ag/AgCl}$) of bio-FET at various concentrations of glucose (1 nM to 1 M) demonstrate that hydrogel gated bio-FET sensor could cause the generation of negative charges rather than conformation change of peptide after exposure to glucose (Fig. S11), resulting in depleting the electrons in metal oxide channel and reducing conductance (Fig. 3c). Therefore, the transfer curve was shifted positively with the increase of [glucose]. The results in Fig. 3d

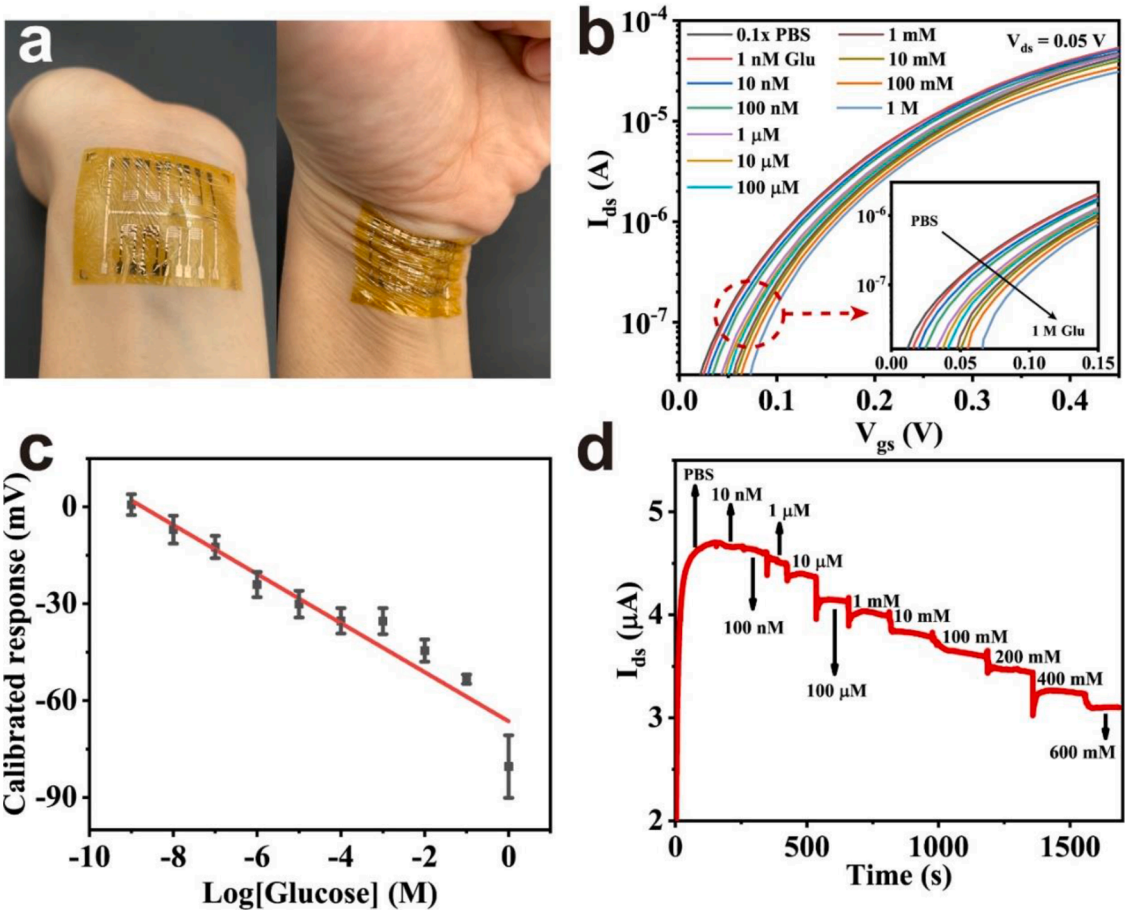

Fig. 4. (a) Optical image of flexible In_2O_3 FET arrays attached on human wrist. The left illustrates a flat state and the right is a bending status. (b) The representative ($n = 3$) of transfer curves of the flexible devices in response to glucose. (c) The relationship between the sensor response and glucose from three devices. (d) Real-time glucose monitoring by the hydrogel gated flexible In_2O_3 FETs. The concentration of glucose ranges from 10 nM to 600 mM.

illustrated that the hydrogel gated bio-FET exhibited a linear relationship between the sensor response shifts and [glucose] in logarithmic scale with a sensitivity of 15.5 mV dec^{-1} and R^2 of 99.4%. Typically, the minimum detectable of this biosensor was 1 nM. We also found that the sensor signal of the hydrogel-gated FETs without boric acid group and bare In_2O_3 devices had no obvious response at different glucose concentrations, confirming the importance of boric acid group (Fig. S12 and 3d).

To further investigate the sensitivity of the hydrogel gated In_2O_3 FET, we performed output characteristics (Fig. S13) with a distinctive pinch-off performance at various [glucose] ranging from 1 nM to 1 M, where the saturation drain currents improved with the decrease of [glucose] (generation of boronate anions). Fig. S14 plotted the real-time monitoring of sensing response as a function of [glucose], where the drain currents dropped instantly by adding glucose electrolyte solution with accumulated concentration into 0.1×PBS buffer, illustrating that hydrogel encoded device exhibits fast response to the glucose. The drift phenomenon refers to a typical characteristic parameter existing in the whole bio-sensing measurements process [41]. Fig. S15 indicates that the hydrogel gated device displayed a more stable performance than the native In_2O_3 device for transfer characteristics in high ion ionic-strength conditions (10 mM glucose solution). The V-T measurement system is utilized to define the drift rate of the sensing device in complex media. Remarkably, the hydrogel gated bio-FET exhibits a low drift effect of only 6.5 mV h^{-1}, which is twice lower than the native device (14.5 mV h^{-1}), suggesting the hydrogel layer on the device could protect the semiconductor layer from ion migration and water invasion.

We next investigate the devices' generalizability in the complex matrix by detecting glucose in mouse serum, where mouse serum-containing glucose is added to the device with [glucose] across the diabetes-related range (0 ~ 30 mM). The results (Fig. 3e and 3f) indicate a positive shift in the transfer curve is obtained after each mouse serum-containing glucose addition over the full range of [glucose] (0 ~ 50 mM), suggesting the robustness of our device for detecting the analytes in complex conditions (Fig. S10). However, compared to PBS buffer, the sensitivity of biosensor tested in mouse serum (27.3 mV dec^{-1}) was relatively higher than PBS environment (15.5 mV dec^{-1}), while the linearity in mouse serum (84.4%) was lower than PBS solution (99.4%), which may be caused by non-specific adsorption of interference in serum.

3.3. *Electrical performances of the hydrogel gated flexible In_2O_3 bio-FETs*

Conformably attaching the device on soft skin surface is essential for further wearable applications [42]. To explore the feasibility of our device in flexible electronics, we fabricated the hydrogel layer on In_2O_3 bio-FETs on polyimide (PI) substrates (~2.9 μm thick, Fig. S16). According to previous reported paper, the flexible device depicts excellent mechanical robustness [34]. The results (Fig. 4a) show that the formed flexible In_2O_3 bio-FET arrays could attach on the human wrist in flat and bending status, demonstrating that the flexible device can conformably be applied to the human wrist. Transfer characteristics (I_{ds}-V_{gs}) of flexible In_2O_3 bio-FET measured in 1 M glucose solution exhibited improved electrical performance with lower *SS* (60.4 mV dec^{-1}), and larger $I_{on/off}$ (1.0×10^3) (Fig. S17). The family of typical transfer curves suggests (Fig. 4b) that the performance of characteristic shifts corresponds

positively with the increase of [glucose]. The flexible device exhibits a linear dependence between V_{th} and [glucose] in a logarithmic scale with a sensitivity of 7.6 mV dec^{-1} and linearity of 93% (Fig. 4c). The sensitivity of the flexible sensor (7.6 mV dec^{-1}) is lower than the rigid device (15.5 mV dec^{-1}), owing to the unevenness of the flexible substrate. Moreover, time-related decreases in drain current (I_{ds}) are obtained with the improvement of [glucose] in all concentration ranges (10 nM to 600 mM), in which the trend is the same as the rigid substrates (Fig. 4d). These results demonstrate the feasibility of the hydrogel-gated flexible device for glucose monitoring.

4. Conclusion

In summary, this work introduces the surface-assisted self-assembly of peptides to form a glucose-specific hydrogel layer on In_2O_3 bio-FETs. The results demonstrated that the surface localized self-assembly of peptides is an effective approach to achieve real-time detection of the biological analytes in complex conditions. Moreover, flexible peptidic hydrogel gated bio-FETs have been demonstrated for wearable glucose detection. Our approach of utilizing peptide-modified bio-FETs could be further explored for detecting a broad of important biological analytes by customizing the recognizing motifs in assembled peptide structures.

Supplementary materials

Supplementary material associated with this article can be found, in the online version, at doi:

CRediT authorship contribution statement

Tengyan Xu: Visualization, Methodology, Formal analysis, Writing – original draft. **Huihui Ren:** Visualization, Methodology, Formal analysis, Writing – original draft. **Yu Fang:** Formal analysis, Writing – review & editing. **Kun Liang:** Methodology, Resources, Writing – review & editing. **Hongyue Zhang:** Formal analysis, Writing – review & editing. **Dingwei Li:** Methodology, Resources, Writing – review & editing. **Yitong Chen:** Methodology, Resources, Writing – review & editing. **Bowen Zhu:** Conceptualization, Supervision, Funding acquisition, Writing – review & editing. **Huaimin Wang:** Conceptualization, Supervision, Funding acquisition, Writing – review & editing.

Declaration of Competing Interest

The authors declare that they have no known competing financial interests or personal relationships that could have appeared to influence the work reported in this paper.

Data availability

Data will be made available on request.

Acknowledgments

H.M. Wang acknowledges the financial support from the National Natural Science Foundation of China (82022038), and Westlake Education Foundation. B.W. Zhu acknowledges the financial support from the National Natural Science Foundation of China (62174138). We thank the Instrumentation and Service Center for Molecular Sciences, Physical Sciences, Westlake Center for Micro/Nano Fabrication, and Biomedical Research Core Facilities at Westlake University for the facility support and technical assistance We thank Jiye Li and Momo Zhao for schematic drawing.

Supplementary materials

Supplementary material associated with this article can be found, in the online version, at doi:10.1016/j.apmt.2022.101713.

References

[1] D.R. Kauffman, A. Star, Electronically monitoring biological interactions with carbon nanotube field-effect transistors, Chem. Soc. Rev. 37 (6) (2008) 1197–1206.
[2] M.J. Schoning, A. Poghossian, Recent advances in biologically sensitive field-effect transistors (BioFETs), Analyst 127 (9) (2002) 1137–1151.
[3] H.H. Bay, R. Vo, X. Dai, H.H. Hsu, Z. Mo, S. Cao, W. Li, F.G. Omenetto, X. Jiang, Hydrogel gate graphene field-effect transistors as multiplexed biosensors, Nano Lett. 19 (4) (2019) 2620–2626.
[4] X. Du, Y. Li, J.R. Motley, W.F. Stickle, G.S. Herman, Glucose sensing using functionalized amorphous in-Ga-Zn-O field-effect transistors, ACS Appl. Mater. Interfaces 8 (12) (2016) 7631–7637.
[5] B. Yu, N. Long, Y. Moussy, F. Moussy, A long-term flexible minimally-invasive implantable glucose biosensor based on an epoxy-enhanced polyurethane membrane, Biosens. Bioelectron. 21 (12) (2006) 2275–2282.
[6] K. Liang, D. Li, H. Ren, M. Zhao, H. Wang, M. Ding, G. Xu, X. Zhao, S. Long, S. Zhu, P. Sheng, W. Li, X. Lin, B. Zhu, Fully printed high-performance n-type metal oxide thin-film transistors utilizing coffee-ring effect, Nano Micro Lett. 13 (1) (2021) 164.
[7] K. Liang, H. Ren, D. Li, Y. Wang, Y. Tang, M. Zhao, H. Wang, W. Li, B. Zhu, Fully-printed flexible n-type tin oxide thin-film transistors and logic circuits, J. Mater. Chem. C 9 (35) (2021) 11662–11668.
[8] N. Nakatsuka, K.-.A. Yang, J.M. Abendroth, K.M. Cheung, X. Xu, H. Yang, C. Zhao, B. Zhu, Y.S. Rim, Y. Yang, Aptamer–field-effect transistors overcome Debye length limitations for small-molecule sensing, Science 362 (6412) (2018) 319–324.
[9] Y.S. Rim, S.-.H. Bae, H. Chen, J.L. Yang, J. Kim, A.M. Andrews, P.S. Weiss, Y. Yang, H.R. Tseng, Printable ultrathin metal oxide semiconductor-based conformal biosensors, ACS Nano 9 (12) (2015) 12174–12181.
[10] R.A. Street, Thin-film transistors, Adv. Mater. 21 (20) (2009) 2007–2022.
[11] T. de Rond, J. Gao, A. Zargar, M. de Raad, J. Cunha, T.R. Northen, J.D. Keasling, A high-throughput mass spectrometric enzyme activity assay enabling the discovery of cytochrome P450 biocatalysts, Angew. Chem. Int. Ed. 131 (30) (2019) 10220–10225.
[12] D. Rodbard, Continuous glucose monitoring: a review of successes, challenges, and opportunities, Diabetes Technol. Ther. 18 (2016) 3–13.
[13] K. Dhara, D.R. Mahapatra, Electrochemical nonenzymatic sensing of glucose using advanced nanomaterials, Mikrochim. Acta 185 (1) (2017) 49.
[14] S.J. Updike, G.P. Hicks, The enzyme electrode, Nature 214 (5092) (1967) 986–988.
[15] J. El-Maiss, M. Cuccarese, C. Maerten, P. Lupattelli, L. Chiummiento, M. Funicello, P. Schaaf, L. Jierry, F. Boulmedais, Mussel-inspired electro-cross-linking of enzymes for the development of biosensors, ACS Appl. Mater. Interfaces 10 (22) (2018) 18574–18584.
[16] Y.S. Rim, H. Chen, B. Zhu, S.H. Bae, S. Zhu, P.J. Li, I.C. Wang, Y. Yang, Interface engineering of metal oxide semiconductors for biosensing applications, Adv. Mater. Interfaces 4 (10) (2017), 1700020.
[17] S. Kim, D.W. Kwon, R. Lee, D.H. Kim, B.G. Park, Investigation of drift effect on silicon nanowire field effect transistor based pH sensor, Jpn. J. Appl. Phys. 55 (6S1) (2016) 06GG01.
[18] J. Wang, Electrochemical glucose biosensors, Chem. Rev. 108 (2) (2008) 814–825.
[19] J.S. Mohammed, W.L. Murphy, Bioinspired design of dynamic materials, Adv. Mater. 21 (23) (2009) 2361–2374.
[20] G. Demirel, F. Buyukserin, Surface-induced self-assembly of dipeptides onto nanotextured surfaces, Langmuir 27 (20) (2011) 12533–12538.
[21] D.G. Anderson, J.A. Burdick, R. Langer, Smart biomaterials, Science 305 (5692) (2004) 1923–1924.
[22] C. Ren, J. Zhang, M. Chen, Z. Yang, Self-assembling small molecules for the detection of important analytes, Chem. Soc. Rev. 43 (21) (2014) 7257–7266.
[23] C. Vigier-Carrière, F. Boulmedais, P. Schaaf, L. Jierry, Surface-assisted self-assembly strategies leading to supramolecular hydrogels, Angew. Chem. Int. Ed. 57 (6) (2018) 1448–1456.
[24] A.M. Bieser, J.C. Tiller, Surface-induced hydrogelation, Chem. Commun. 31 (2005) 3942–3944.
[25] S. Kiyonaka, K. Sada, I. Yoshimura, S. Shinkai, N. Kato, I. Hamachi, Semi-wet peptide/protein array using supramolecular hydrogel, Nat. Mater. 3 (1) (2004) 58–64.
[26] X. Wang, X. Yu, X.S. Wang, M.Y. Qi, J. Pan, Q.G. Wang, One-step nanosurface self-assembly of D-peptides renders bubble-free ultrasound theranostics, Nano Lett. 19 (4) (2019) 2251–2258.
[27] D. Spitzer, V. Marichez, G.J.M. Formon, P. Besenius, T.M. Hermans, Surface-assisted self-assembly of a hydrogel by proton diffusion, Angew. Chem. Int. Ed. 57 (35) (2018) 11349–11353.
[28] H. Wang, J. Shi, Z. Feng, R. Zhou, S. Wang, A.A. Rodal, B. Xu, An *in situ* dynamic continuum of supramolecular phosphoglycopeptides enables formation of 3D cell spheroids, Angew. Chem. Int. Ed. 56 (51) (2017) 16297–16301.
[29] W. Zheng, J. Gao, L. Song, C. Chen, D. Guan, Z. Wang, Z. Li, D. Kong, Z. Yang, Surface-induced hydrogelation inhibits platelet aggregation, J. Am. Chem. Soc. 135 (1) (2013) 266–271.
[30] J.R. Fores, M. Criado-Gonzalez, A. Chaumont, A. Carvalho, C. Blanck, M. Schmutz, C.A. Serra, F. Boulmedais, P. Schaaf, L. Jierry, Supported catalytically active

supramolecular hydrogels for continuous flow chemistry, Angew. Chem. Int. Ed. 58 (52) (2019) 18817–18822.
[31] M.G. Kim, M.G. Kanatzidis, A. Facchetti, T.J. Marks, Low-temperature fabrication of high-performance metal oxide thin-film electronics via combustion processing, Nat. Mater. 10 (5) (2011) 382–388.
[32] Y.S. Rim, H.J. Chen, Y.S. Liu, S.H. Bae, H.J. Kim, Y. Yang, Direct light pattern integration of low-temperature solution-processed all-oxide flexible electronics, ACS Nano 8 (9) (2014) 9680–9686.
[33] D.W. Li, M.M. Zhao, K. Liang, H.H. Ren, Q.T. Wu, H. Wang, B.W. Zhu, Flexible low-power source-gated transistors with solution-processed metal-oxide semiconductors, Nanoscale 12 (42) (2020) 21610–21616.
[34] H. Ren, T. Xu, K. Liang, J. Li, Y. Fang, F. Li, Y. Chen, H. Zhang, D. Li, Y. Tang, Y. Wang, C. Song, H. Wang, B. Zhu, Self-assembled peptides-modified flexible field-effect transistors for tyrosinase detection, iScience 25 (1) (2022), 103673.
[35] Z. Feng, H. Wang, R. Zhou, J. Li, B. Xu, Enzyme-instructed assembly and disassembly processes for targeting downregulation in cancer cells, J. Am. Chem. Soc. 139 (11) (2017) 3950–3953.
[36] X.J. Yang, H.L. Lu, Y.H. Tao, L.C. Zhou, H.M. Wang, Spatiotemporal control over chemical assembly in living cells by integration of acid-catalyzed hydrolysis and enzymatic reactions, Angew. Chem. Int. Ed. 60 (44) (2021) 23797–23804.
[37] J. Wang, L.B. Hu, H.Y. Zhang, Y. Fang, T.L. Wang, H.M. Wang, Intracellular condensates of oligopeptide for targeting lysosome and addressing multiple drug resistance of cancer, Adv. Mater. 34 (1) (2022).
[38] J. Yan, H. Fang, B. Wang, Boronolectins and fluorescent boronolectins: an examination of the detailed chemistry issues important for the design, Med. Res. Rev. 25 (5) (2005) 490–520.
[39] T. Kajisa, T. Sakata, Glucose-responsive hydrogel electrode for biocompatible glucose transistor, Sci. Technol. Adv. Mater. 18 (1) (2017) 26–33.
[40] H. Ren, K. Liang, D. Li, M. Zhao, F. Li, H. Wang, X. Miao, T. Zhou, L. Wen, Q. Lu, Interface engineering of metal-oxide field-effect transistors for low-drift pH sensing, Adv. Mater. Interfaces 8 (20) (2021), 2100314.
[41] Y.H. Liao, J.C. Chou, Preparation and characteristics of ruthenium dioxide for pH array sensors with real-time measurement system, Sens. Actuators B Chem. 128 (2) (2008) 603–612.
[42] P. Cai, W.R. Leow, X. Wang, Y.L. Wu, X. Chen, Programmable nano–bio interfaces for functional biointegrated devices, Adv. Mater. 29 (26) (2017), 1605529.